Available online at www.sciencedirect.com
ScienceDirect
Journal of Physics and Chemistry of Solids 68 (2007) 124–130
JOURNAL OF PHYSICS AND CHEMISTRY OF SOLIDS
www.elsevier.com/locate/jpcs

Oxygen vacancy doping effect on the electrical and magnetic behavior of $Ba_{5-x}La_xNb_{4-x}Ti_xO_{15}$

J.M. De Paoli[a], R.E. Carbonio[a,c], R.D. Sánchez[b,c,*]

[a]*INFIQC, Departamento de Físico Química, Facultad de Ciencias Químicas, Universidad Nacional de Córdoba, Ciudad Universitaria, 5000 Córdoba, Argentina*
[b]*Comisión Nacional de Energía Atómica, Centro Atómico Bariloche and Instituto Balseiro, 8400 Bariloche, Argentina*
[c]*CONICET, Argentina*

Received 7 March 2006; received in revised form 19 August 2006; accepted 18 September 2006

Abstract

We report electric and magnetic properties of oxygen deficient $Ba_{5-x}La_xNb_{4-x}Ti_xO_{15-\delta}$ phases, which have been prepared by solid-state reaction method followed by a controlled reduction process under hydrogen atmosphere. The extra electrons added by the formation of the oxygen vacancies (δ) introduce localized spins and the magnetic susceptibility can be described by a temperature-independent contribution and a Curie–Weiss term associated to the Ti^{3+} ion formation. Besides, the experimental resistivity (ρ) data of these four reduced compounds are well described in a wide temperature range with the equation $\rho \approx AT\ \exp(B/T)^{-1/4}$, which suggests the presence of small polarons in the system. Although, all samples present electrical insulating behavior, the electrical resistivity decreases four orders of magnitude for intermediate x values. We interpreted this fact as a consequence of the mix between the localized bands of the Nb and Ti ions, which favors the promotion of carriers due to reduction of the band gap.

Keywords: A. Oxides; D. Electrical conductivity; D. Magnetic properties

1. Introduction

Complex oxides with titanium, tantalum or niobium are compounds with a great technological interest due to the dielectric properties, in particular for future application in wireless communications [1]. Microwave dielectric properties of $Ba_5Nb_4O_{15}$ have been recently studied [2–7] because of their high dielectric constants; low dielectric loss and small temperature coefficient that make this compound a good candidate for dielectric resonators. Luminescent properties have also been informed [8].

On the other hand, reduced phases of binary and complex Ti and Nb oxides have been informed to have superconducting properties at very low temperatures [9–21]. These properties were correlated with those of the superconducting Cu oxides through the so-called, "electron–hole symmetry" [22]; besides, a common property among the copper and noncopper superconductors is the presence of layered structures. Thus, layered reduced titanates and niobates are good candidates to search for new superconducting compounds as suggested by the presence of superconductivity in Li-intercalated layered perovskites $Li_xAB_2Na_{n-3}Nb_nO_{3n+1}$ (A = K, Rb, Cs; B = Ca, Sr, Ba) with $n = 3$ and 4.

$Ba_5Nb_4O_{15}$ is a five layers perovskite compound belonging to the general family of compounds $A_nB_{n-1}O_{3n}$, with $n-1$ corner-sharing octahedra separated by vacant octahedra layers [23–25]. In previous studies, we reported the far-IR reflectivity, Raman spectra [26] and infrared and transport properties of $Ba_5Nb_4O_{15}$ and its oxygen-deficient phases [27]. The reduced $Ba_5Nb_4O_{15-\delta}$ phases were semiconducting with increasing conductivity as δ increased. Moreover far IR-reflectivity revealed that, at the highest vacancy level obtained in Ref. [27] ($\delta = 0.54$), carriers are not free enough to interact with phonon longitudinal

*Corresponding author. Centro Atómico Bariloche, R8402AGP Bariloche, Río Negro, Argentina. Tel.: +54 2944 445158; fax: +54 2944 445299.
E-mail address: rodo@cab.cnea.gov.ar (R.D. Sánchez).

0022-3697/$ - see front matter © 2006 Elsevier Ltd. All rights reserved.
doi:10.1016/j.jpcs.2006.09.015

modes. Activation energies of the order of 10^{-2} eV with decreasing values as δ increased were obtained. It was expected that a metal–insulator transition could be reached at higher number of O vacancies, however with the reducing method used in Ref. [27] it was impossible to obtain values of δ larger than 0.54.

In the series $Ba_{5-x}La_xNb_{4-x}Ti_xO_{15}$, only the members with $x = 0$ and $x = 4$ have been previously studied by other authors [28–31]. In the particular case of $x = 4$, its structure was refined with neutron powder diffraction (NPD) [31] as an intergrowth of the $BaTiO_3$–$La_4Ti_3O_{12}$ system. The fact that Ti^{4+} is easier to reduce than Nb^{5+} impelled us to replace Nb^{5+} by Ti^{4+} in $Ba_5Nb_4O_{15}$ and in order to keep electroneutrality Ba^{2+} was replaced by La^{3+}.

We have recently reported the synthesis and structural characterization of the whole solid solution $Ba_{5-x}La_xNb_{4-x}Ti_xO_{15}$ using high-resolution NPD [32]. We found that La^{3+} occupies preferentially the A2 site (Wyckoff site 2d) and Ti^{4+} the B2 site (Wyckoff site 2c). As x increases there is an increase of the global instability index (GII) (which is a measure of the extent to which the bond valence rule is violated over the whole structure) indicating the presence of intrinsic strains large enough to cause instability at room temperature. This strain is responsible for a structural change from space group P-3m1 for the $x = 0$, 1 and 2 members (stacking sequence chhcc, polytypoid 5H) to space group P-3c1 for the member with $x = 3$ (stacking sequence $(chhcc)_2$, polytypoid $2 \times 5H = 10H$). This change in space group is associated with a cooperative rotation of $(Nb/Ti)O_6$ octahedra around the c-axis, necessary to accommodate the smaller La^{3+} ion in the cuboctahedral cavity.

This paper reports on the synthesis of reduced phases $Ba_{5-x}La_xNb_{4-x}Ti_xO_{15-\delta}$ ($x = 1$, 2, 3 and 4) and their electric and magnetic characterization. Additionally, we propose a band scheme to explain the observed behavior.

2. Experimental

$Ba_{5-x}La_xNb_{4-x}Ti_xO_{15}$ ($x = 1$, 2, 3 and 4) were obtained by solid-state reaction method, using La_2O_3 (previously treated at 900 °C in air in order to eliminate hydration), $BaCO_3$, Nb_2O_5 and TiO_2. They were mixed, ground, and treated at 1300 °C for 12 h in air. The resulting powder was reground and calcined at the same temperature for 12 h, then re-heated at 1500 °C for 12 h. A slow cooling process from 1500 to 900 °C was essential to obtain single-phase lanthanum/titanium-containing compounds. The reduced phases, $Ba_{5-x}La_xNb_{4-x}Ti_xO_{15-\delta}$ ($x = 1$, 2, 3 and 4 and $\delta < 0.15$), were obtained from the oxidized samples by reduction in a 5% H_2 + 95% Ar atmosphere at 1300 °C. δ values were estimated by the mass change in the re-oxidation of the reduced compounds in air at 1300 °C. The δ values obtained according to this procedure present an important error but these are approximately between $\delta \approx 0.04$ and 0.10 depending on the sample. These oxygen dopings introduce 2–10% of electrons by B site. All values are quite small and they do not change monotonically with x. X-ray diffraction patterns were used to corroborate that the oxidized phases are recovered after a thermal treatment in oxygen atmosphere.

The structural characterization of the samples was carried out by laboratory XRPD data with a Phillips W1700 powder diffractometer (Cu Kα, $\lambda = 1.5418$ Å) taken between 10° and 100° in 2θ range, with increments of 0.02° and a counting time of 10 s. The FULLPROF program [33] was used to refine the crystal structure by the Rietveld method. A pseudo-Voigt shape function was always adequate to obtain good fits. During the refinements, the atomic positions temperature factors and occupancies were kept constant to the values obtained from the NPD refinements for the oxidized phases [32], only profile and cell parameters were refined.

The electrical resistivity was measured, in the temperature range 10–300 K using four-probe method on sintered pellets in a commercial cryostat.

The DC magnetization was measured with a commercial superconducting quantum interference device magnetometer on powdered samples, in the temperature range 10–300 K and magnetic field of 5 kOe.

3. Results and discussion

3.1. Structural characterization

The refined XRPD powder patterns for the reduced phases with $x = 1$ and 3 (using the space groups P-3m1 and P-3c1, respectively), are shown in Fig. 1. The obtained discrepancy factors are, for $x = 1$: $R_p = 12.7\%$, $R_{wp} = 15.7\%$, $R_I = 5.04\%$ and $\chi^2 = 2.52$; and for $x = 3$: $R_p = 10.9\%$, $R_{wp} = 14.2\%$, $R_I = 5.98\%$ and $\chi^2 = 3.88$. General representations of these crystal structures are shown in Fig. 2.

These good refinements show that the oxygen-deficient phases have the same crystal structures than those of the parent oxidized compounds [32].

The dependence of cell parameters with x is shown in Fig. 3. A decrease in the unit cell parameters as x increases is observed, which is consistent with the smaller ionic radii of cuboctahedral $^{XII}La^{3+}$ (1.36 Å) compared to cuboctahedral $^{XII}Ba^{2+}$ (1.61 Å). Two linear regions are observed for the c parameter, corresponding to the two space groups.

3.2. Magnetic properties

The magnetic susceptibility χ was taken as the ratio between the magnetization M and the magnetic field H. For the oxygen-stoichiometric compounds we observed diamagnetic behavior (see the inset of Fig. 4) because all ions have the electronic configuration of the preceding noble gas; the core expected contributions (χ_{diamag}) are shown in the second column of Table 1. Stoichiometric

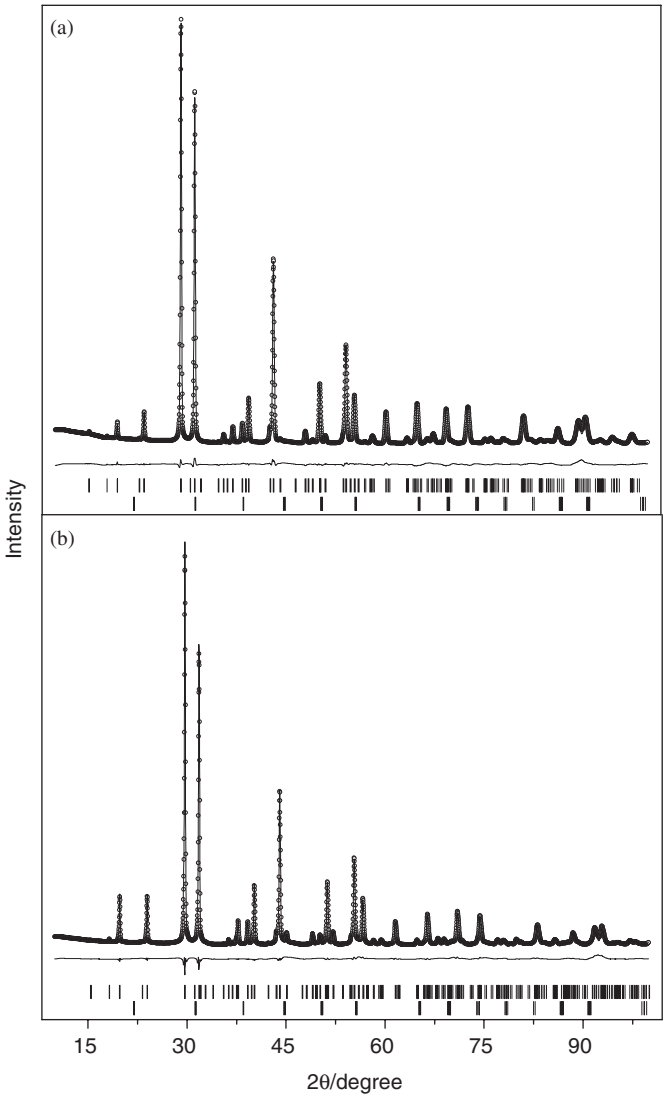

Fig. 1. Observed (circles), calculated (solid line) and difference (at the bottom) X-ray powder diffraction taken at room temperature, for: (a) $Ba_4LaNb_3TiO_{15-\delta}$, refined in the space group P-3m1 and (b) $Ba_2La_3NbTi_3O_{15-\delta}$, refined in the space group P-3c1. Upper set of vertical marks correspond to the position of the allowed Bragg reflections of the main phase, lower ones correspond to $BaTiO_3$ (space group P4/mmm) obtained as impurity (less than 9%).

samples are consequently diamagnetic; however, oxygen vacancies introduce electrons into the system, presumably forming Ti^{3+} ([Ar] $3d^1$) cations because of the Ti^{4+} facility to reduce its oxidation state in comparison with Nb^{5+} ions. In any case, we can assume that the extra electrons, with $S=\frac{1}{2}$, are localized on the B sites. Subtracting the diamagnetic susceptibility to the experimental data and normalizing the values by mol of B site we obtain the temperature dependence of χ that is shown in Fig. 4. It is surprising the coincidence between the curves with $x=1$ and 2 and those with $x=3$ and 4, respectively. All of them, at low temperature, clearly present a Curie tail, which confirms the presence of the extra localized electrons in the system.

In the bottom of Fig. 4, we represent the reciprocal susceptibility χ^{-1}. Note the nonlinearity of the χ^{-1} vs. T curves, instead of the expected Curie law for a paramagnetic system. In order to describe the experimental curves we considered two contributions through the equation: $\chi^{-1}=(xC/(T-\Theta)+\chi_0)^{-1}$. One of them is the term $xC/(T-\Theta)$, where x is the B site fraction with an extra electron. C is the Curie constant, corresponding to paramagnetic electrons with $S=\frac{1}{2}$, and Θ is the Curie–Weiss temperature. The second, χ_0, is an extra term, which takes into account a temperature-independent contribution (TIC). Parameters obtained from the fits are shown in columns 2–4 of Table 1. Solid lines in Fig. 4 show the fitting of the data. Note that the % of occupied B sites with $S=\frac{1}{2}$ (see column 5 of Table 1) are in agreement with the range of the δ values obtained after the re-oxidation process of the samples. Similar temperature behavior and values of χ_0 were observed in Ti_3O_5 with low values of V doping [34].

Although the reductions introduce practically the same amount of extra electrons to the titanium atoms for all the compounds, it is very interesting to remark the superposition of some of the magnetic susceptibility curves. In the upper panel of Fig. 4, at high temperatures, it is easy to see how the $x=1$ and the $x=2$ data tend asymptotically to the same χ_0 value (see Table 1). The same tendency occurs with the $x=3$ and $x=4$ susceptibility data. Essentially, this effect occurs because these two sets of samples present different space group symmetry (P-3m1 and P-3c1, respectively), and consequently different distortions of the oxygen octahedra around the metal transition ions. These distortions strongly affect the crystal field around the Ti^{3+} ions and consequently change the magnitude of the TIC magnetic susceptibility contribution.

3.3. Electrical properties

In Fig. 5 we show electrical resistivity ρ vs. temperature. All samples show insulating behavior. Here we call the attention that at low temperatures, the sample with $x=2$ presents lower resistivity ($\sigma \approx 0.02\,\Omega^{-1}\mathrm{cm}^{-1}$). For $x=1$, 2 and 3, one can clearly see a change of regime at approximately $T^*=120$, 240 and 150 K, respectively. Thus, at low temperature ρ tends to a finite value and at high temperature is apparently a semiconductor, whose expected behavior is $\rho=\rho_0\exp(E_g/kT)$ where E_g is the gap between bands. To corroborate this thermal activation process we plot the data as $\ln\rho$ vs. T^{-1} (shown in the inset at the bottom of Fig. 5, for $x=4$). However, we can see that the resistivity does not follow an Arrhenius dependence. Above T^*, the samples with $x=1$, 2 and 3 present very similar deviations of ρ(T) with respect the expected behavior. However, in order to estimate the magnitude of the band gap, at high temperatures we obtained E_g values of 63, 30 and 72 meV for $x=1, 2$ and 3, respectively.

In order to explore the transport mechanism involved in this system, we estimate the scaled temperature derivative

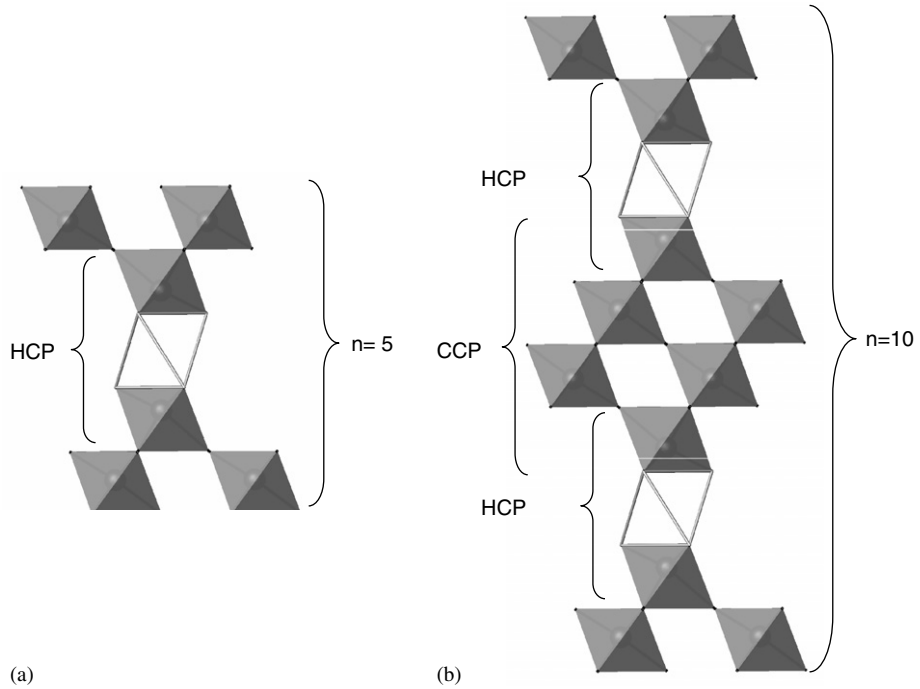

Fig. 2. General representation of the structure of the $Ba_{5-x}La_xNb_{4-x}Ti_xO_{15}$ ($x = 0$, 1, 2, 3 and 4) compounds, viewed along the [0 0 1] direction. (a) Polytypoid 5H (chhcc) corresponding to the crystalline structure for $x = 0$, 1 and 2 compounds, and (b) Polytypoid 10H (chhcchhcc) corresponding to the crystalline structure for $x = 3$ and 4 compounds. Gray octahedra: $(Nb/Ti)O_6$ sites, light gray spheres: B type cations. A type cations and O^{2-} anions are omitted for simplification.

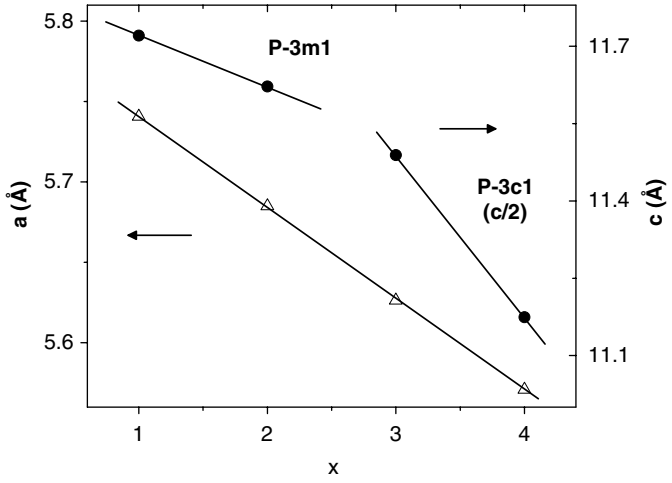

Fig. 3. Cell parameters for the $Ba_{5-x}La_xNb_{4-x}Ti_xO_{15-\delta}$ oxygen-deficient phases. △: parameter a; ●: parameter c for space group P-3m1 and c/2 for P-3c1.

(STD) of the resistivity, $(1/\rho)\,(d\rho/dT)$. We plot the STD temperature dependence in Fig. 6 for $x = 1$, 2 and 3. The negative values also indicate that the samples are insulators for all the explored temperature range. At low T, $T < T^*$, low values can be observed, indicating the small temperature dependence of the carrier mobility. Notably, near T^*, STD progressively decreases in magnitude to reach practically a constant value. This described behavior supports the idea that at least two regimes govern the electrical resistivity, which clearly can be seen at low and at high temperature, respectively. The small temperature dependence of the carrier mobility at low temperature resembles the behavior of doped semiconductors by the nearest-neighbor hopping process. Fitting the data, below T^* using the equation $\rho = \rho_0 \exp(\varepsilon/kT)$, we obtained small values of activation energy ($\varepsilon \sim 0.35$ meV). On the other hand, in insulating materials as $SrTiO_3$, oxygen deficiencies can introduce small concentrations of free electrons which form a degenerate gas in the d band of Ti. In this case, the conductivity tends to a finite value at low temperatures and it is well known that small polarons can be formed [35,36]. From the magnetic susceptibility data, the concentration of localized electrons formed by the reduction process permits to determine the carrier concentration ($n = 5 \times 10^{20}\,\mathrm{cm}^{-3}$). Using the equation $n^{1/3}a_H \approx 0.26$, the hydrogen radius a_H between the positive charge and the polaron is 2.5 Å.

At high temperature, if we associate $\ln\rho$ vs. T^{-1} data with the formula $\rho(T) = \rho_0 \exp(E_g(T)/kT)$, we can differentiate the experimental data, obtaining $E_g(T) = \mathrm{d}(\ln\rho)/\mathrm{d}T^{-1}$ vs. T. These are plotted in the bottom of Fig. 6. Now, we can observe how at low temperature, below T^*, E_g is practically constant ($E_g \sim \varepsilon$) and with a small value, while, at approximately T^*, E_g starts to increase linearly with T. Our results suggest that $\rho(T)$, between T^* and room temperature approximately, can be described as a semiconductor with a temperature-dependent gap $E_g(T)$. In titanates such as Ti_2O_3 with corundum structure, the lack of stoichiometry dopes the system as an intrinsic

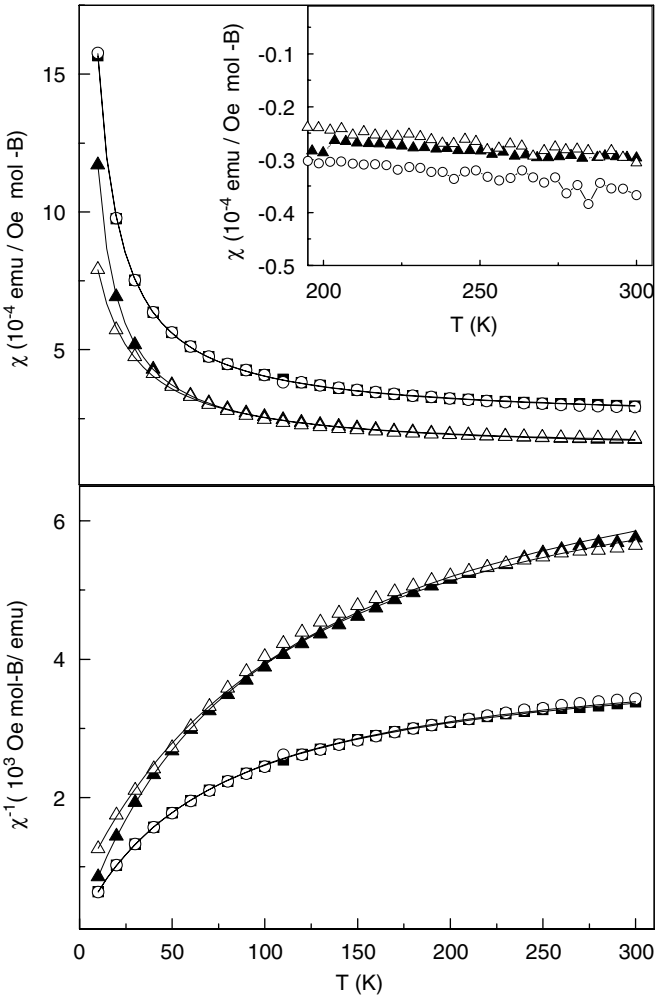

Fig. 4. Upper plot: the magnetic susceptibility vs. temperature of the $x = 1, 2, 3$ and 4, taken at 5 kOe for oxygen-reduced samples. The susceptibilities of oxidized samples are in the inset. In the bottom: the inverse of the susceptibilities of reduced samples where it can be seen the deviation of the Curie expected behavior. ■: $x = 1$; ○: $x = 2$; ▲: $x = 3$ and △: $x = 4$.

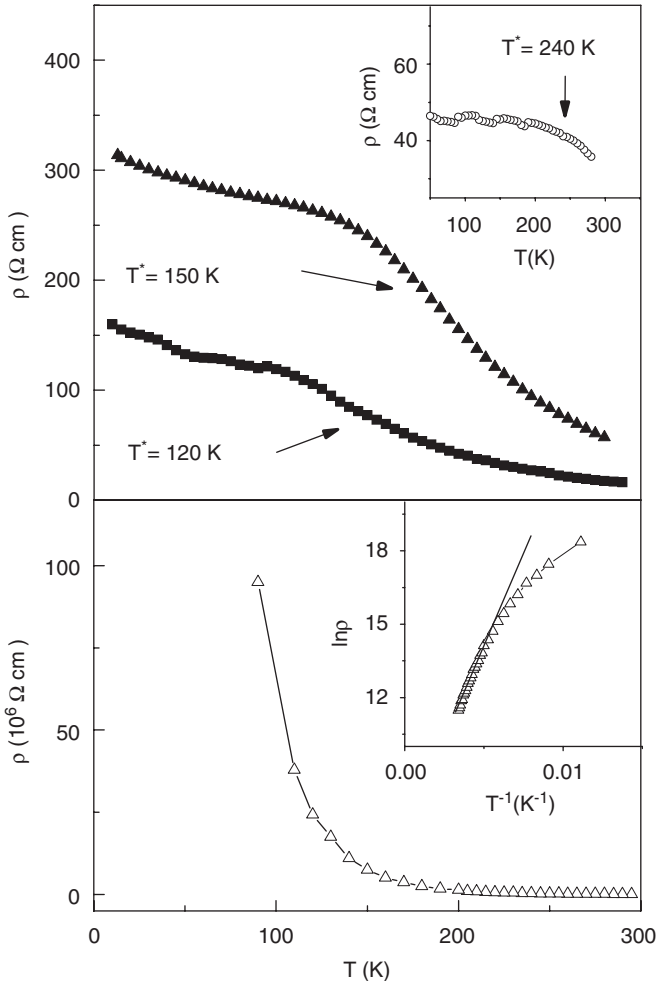

Fig. 5. Upper plot: Temperature dependence of the electrical resistivity for $x = 1$ and 3 samples, and in the inset for $x = 2$. T^* indicates the temperature at which a change of behavior is observed. In the bottom: electrical resistivity vs. T for $x = 4$. In the inset, $\ln\rho$ vs. T^{-1} for $x = 4$. ■: $x = 1$; ○: $x = 2$; ▲: $x = 3$ and △: $x = 4$.

Table 1
Fitted magnetic parameters for the compounds $Ba_{5-x}La_xNb_{4-x}Ti_xO_{15-\delta}$ ($x = 1, 2, 3$ and 4)

Sample	$-\chi_{diamag}$ (10^6 emu/mol Oe)	χ_0 (10^{-4} emu/mol-B Oe)	$-\Theta$ (K)	xC (emu K/mol-B Oe)	Occupancy of B site with $S = \frac{1}{2}$ (%)
$x = 1$	360	2.40 (3)	2.7 (1)	0.0168 (1)	8
$x = 2$	344	2.40 (3)	2.6 (1)	0.0169 (1)	8
$x = 3$	328	1.30 (3)	2.0 (1)	0.0124 (1)	6
$x = 4$	312	1.20 (2)	11.6 (5)	0.0144 (3)	7

semiconductor and the activation energy in the conductivity does not appears to be constant [37,38].

Finally, to clarify which mechanism is present at low temperature, below T^*, we fitted the data with several expressions, including interacting electrons with the phonons of the lattice (polarons). We obtained the best fit adjusting with the expression: $\rho(T) = AT\exp(T_0/T)^{-1/4}$. This corresponds to the description of conductivity of small polarons, characterized by a T dependence of the pre-exponential factor, which are thermally activated by variable range hopping (VRH) between localized states, polaron-VRH [39]. In Fig. 7 we plot $\ln(\rho/T)$ vs. $T^{-1/4}$ data and the solid lines represents the best fits below T^*. This is an interesting result because the electron in a Ti^{3+} has an important electron–phonon interaction, maybe with local octahedron distortion, which jumps to the nearest Ti^{4+} neighbor between localized states of the band. Within this hopping model between localized states, T_0 is a parameter that relates the localization length of the electron, ξ. The relation between them is $k_B T_0 \approx 2.8(e^2/\kappa\xi)$ [36], where κ is the dielectric constant and 2.8 is a numerical factor. From these estimations we used $\kappa = 10$, but a more precise value will depend on the knowledge of κ. From the fits we obtain T_0 values around 21,000 K for $x = 1$, 2 and 3, which gives $\xi \approx 2.2$ Å. Similar values were observed in manganites [40].

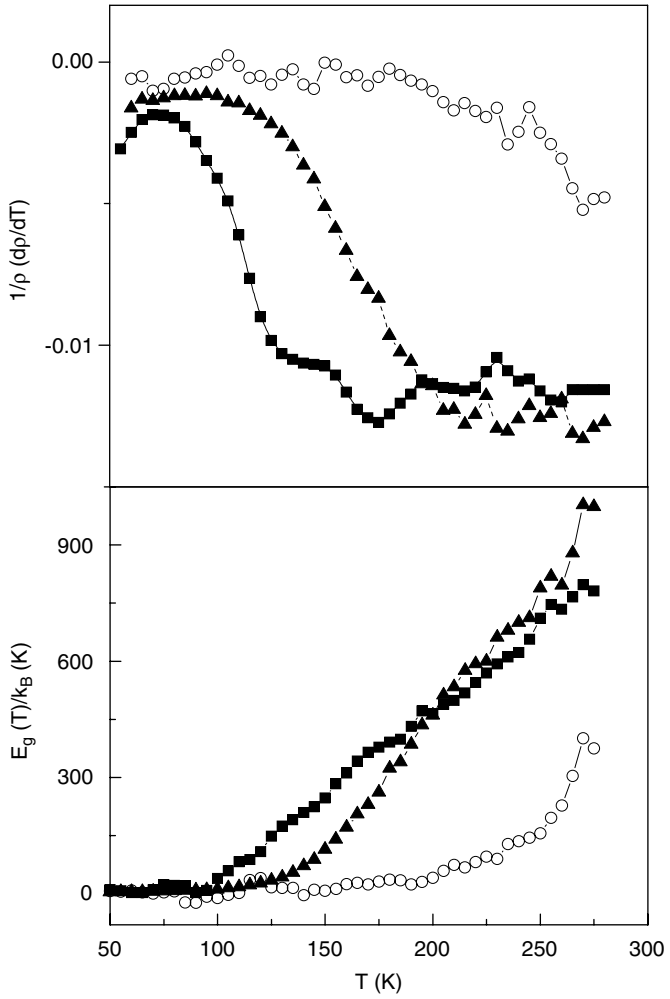

Fig. 6. For $x = 1, 2$ and 3 samples, the upper figure shows the temperature dependence of the STD of the resistivity, $(1/\rho)(d\rho/dT)$. The bottom figure is the $d(\ln \rho)/(dT^{-1})$ vs. T showing temperature dependence of the gap. ■: $x = 1$; ○: $x = 2$ and ▲: $x = 3$.

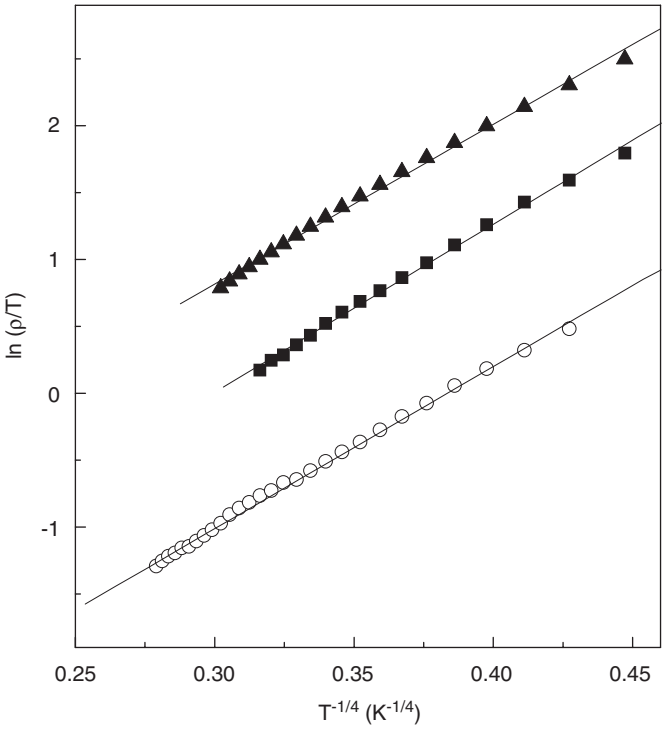

Fig. 7. ln (ρ/T) vs. $T^{-1/4}$ below T^* for $x = 1$, 2 and 3 samples. The solid lines indicate the best linear fits. ■: $x = 1$; ○: $x = 2$ and ▲: $x = 3$.

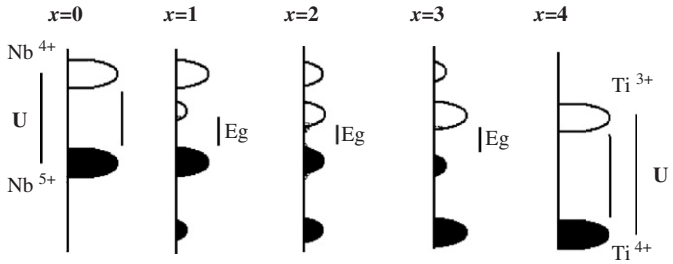

Fig. 8. Bands scheme for the extreme compositions ($x = 0$, only Nb, and $x = 4$, only Ti in the B sites). Also is represented the situation for the intermediate compositions ($x = 1$, 2 and 3).

Also, this localization length value is in excellent accord with our previous estimation of a_H.

An interesting point to mention is that the sample with $x = 4$ has the resistivity four orders of magnitude higher than the $x = 1$, 2 and 3 samples. In this set of samples, other interesting observation is to consider the minima in ρ and δ for the $x = 2$ composition. The B sites of the $x = 4$ sample, without Nb, are occupied by Ti ions and if one of the extra electrons jumps to the nearest Ti neighbor, we can use the ionic model [41] to estimate the magnitude of this excitation gap, $U_{Ti} = I(Ti^{4+}) - I(Ti^{3+}) - (e^2/d_{Ti-Ti})$, where $I(Z^{n+})$ is the ionization potential of the Z^{n+} ion. For this case we estimate the gap between the two metallic bands in 12 eV. Similar reasoning can be made for the other extreme, $x = 0$ with only Nb ions in the B sites, and the gap in this case is around 8 eV. These values normally are overestimated because screening and others effects have not been taken into account. The explanation of the low resistivities of the set with $x = 1$, 2 and 3 is that two Nb and the two Ti bands are superimposed, reducing thus the energy gap notably for the excitations. Practically, $x = 1$ and 3 present a symmetric behavior. In the first case the Ti band plays the role of impurities in a semiconductor and in the second composition, the impurity band is due to the Nb ions. The experimental observations are consistent with the band scheme proposed (see Fig. 8), the impurity band ($x = 1$, 2 and 3) reduces notably the gap, and consequently the electrical resistivity drops four orders of magnitude.

At low temperature the predominant mechanism is due to the hopping of polarons between localized states (polaron-VRH), which are below one mobility edge (E_c), while at high temperature the electrons are thermally promoted from the full metal band to above E_c of the empty impurity band. Finally, comparing the similar resistivities of $x = 1$, 2 and 3, the minimum of $x = 2$ at low T can be explained invoking a small shift of the edge of

mobility by an increase of the bandwidth. This is supported with the structural observation, where the bending of the B–O–B angle in the $x = 2$ sample is more near 180° than the corresponding for $x = 1$ and $x = 3$ [32]. This effect results in an enhancement of the bandwidth with possibly a shift of E_c, which reduces the effective gap of the $x = 2$ system with respect to both the side compositions.

4. Conclusions

From this study we can get the following conclusions. The temperature independent susceptibility term is well consistent with magnetic systems where the first excited level is at approximately $100\,cm^{-1}$ of the ground state. Rising temperature populates the excited state and the magnetic susceptibility shifts from a Curie dependence towards a constant value. This observation confirms the first hypothesis that the doped electrons added by the reduction process forms Ti^{3+} in the system. The low and negative Θ temperatures suggest that small antiferromagnetic coupling exists between two neighboring electrons.

All the studied compounds are insulators but the resistivity of the intermediate composition (B = Ti and Nb) is lower than one of the end members of the series (B = Ti). The replacements of Nb by Ti ions introduce a new set of bands, which acts as a donor impurity band, explaining the decrease of the resistivity when both Ti and Nb ions coexist in the structure. Two mechanisms are involved in the electric transport of the intermediate compositions, at low temperature there is a small polaron with variable range hopping between localized states, while at high temperatures a thermally activated semiconducting behavior with a temperature dependent gap is observed.

Acknowledgments

REC and RDS thank ANPCYT (Projects PICT2003 06-15102 and PICT 17-21372, respectively), and CONICET (PIP no. 5767/05 and PIP no. 5250/05, respectively). REC also thanks SECyT-UNC (Project 197/05). RDS also thanks SEPCyT-UNCu (Project 06/C203). J.M. De Paoli thanks CONICET for a fellowship.

References

[1] P.K. Davies, in: T. Negas, H. Ling (Eds.), Materials and Processes for Wireless Communications, American Ceramic Society, Westerville, OH, 1995, pp. 137–151.
[2] C. Vineis, P.K. Davies, T. Negas, S. Bell, Mater. Res. Bull. 31 (1996) 431–437.
[3] R. Ratheesh, M.T. Sebastian, P. Mohanan, M.E. Tobar, J. Hartnett, R. Woode, D.G. Blair, Mater. Lett. 45 (2000) 279–285.
[4] D.W. Kim, K.S. Hong, C.S. Yoon, C.K. Kim, J. Eur. Ceram. Soc. 23 (2003) 2597–2601.
[5] M.T. Sebastian, I.N. Jawahar, P. Mohanan, Mater. Sci. Eng. B 97 (2003) 258–264.
[6] I.N. Jawahar, M.T. Sebastian, P. Mohanan, Mater. Sci. Eng. B 106 (2004) 207–212.
[7] I.N. Jawahar, P. Mohanan, M.T. Sebastian, Mater. Lett. 57 (2003) 4043–4048.
[8] A.M. Srivastava, J.F. Ackerman, W.W. Beers, J. Solid State Chem. 14 (1997) 187–191.
[9] M.J. Geselbracht, T.J. Richardson, A.M. Stacy, Nature 345 (1990) 324.
[10] J. Akimitsu, J. Amano, H. Sawa, O. Nagase, K. Gyoda, M. Kogai, Jpn. J. Appl. Phys. 30 (1991) L1155–L1156.
[11] Y. Takano, S. Takayanagi, S. Ogawa, T. Yamadaya, N. Mori, Solid State Commun. 103 (1997) 215–217.
[12] H. Fukuoka, T. Isami, S. Yamanaka, Chem. Lett. 8 (1997) 703–704.
[13] Y. Takano, H. Taketomi, H. Tsurumi, T. Yamadaya, N. Mori, Physica B 68 (1997) 237–238.
[14] I. Nagai, Y. Abe, M. Kato, Y. Koike, M. Kakihana, Physica C 357–360 (2001) 393–396.
[15] M. Kato, A. Inoue, I. Nagai, M. Kakihana, A.W. Sleight, Y. Koike, Physica C 388–389 (2003) 445–446.
[16] I. Nagai, Y. Abe, M. Kato, Y. Koike, M. Kakihana, Solid State Ion. 151 (2002) 265–268.
[17] J.J. Schooley, W.R. Hosler, L.M. Cohen, Phys. Rev. Lett. 12 (1964) 474–477.
[18] D.C. Johnston, H. Prakash, W.H. Zachariasen, R. Viswanathan, Mater. Res. Bull. 8 (1973) 777–779.
[19] A. Baratoff, G. Binning, Physica B + C 108 (1981) 1335–1336.
[20] P.B. Allen, Solid State Commun. 13 (1973) 411–415.
[21] R.N. Shelton, D.C. Johnston, H. Adrian, Solid State Commun. 20 (1976) 1077–1080.
[22] F. Deslandes, A.I. Nazzal, J.B. Torrance, Physica C 179 (1991) 85–88.
[23] G. Trolliard, N. Teneze, Ph. Boullay, M. Manier, D. Mercurio, J. Solid State Chem. 173 (2003) 91–100.
[24] Ph. Boullay, N. Teneze, G. Trolliard, D. Mercurio, J.M. Perez-Mato, J. Solid State Chem. 174 (2003) 209–220.
[25] G. Trolliard, N. Teneze, Ph. Boullay, D. Mercurio, J. Solid State Chem. 177 (2004) 1188–1196.
[26] N.E. Massa, S. Pagola, R.E. Carbonio, Phys. Rev. B 53 (1996) 8148–8150.
[27] S. Pagola, N.E. Massa, G. Polla, G. Leyva, R.E. Carbonio, Physica C 235–240 (1994) 755–756.
[28] N. Harre, D. Mercurio, G. Trolliard, J.P. Mercurio, Ann. Chim. Sci. Mater. 23 (1998) 233–236.
[29] N. Harre, D. Mercurio, G. Trolliard, B. Frit, Mater. Res. Bull. 33 (1998) 1537–1548.
[30] G. Trolliard, N. Harre, D. Mercurio, B. Frit, J. Solid State Chem. 145 (1999) 678–693.
[31] N. Teneze, D. Mercurio, G. Trolliard, B. Frit, Mater. Res. Bull. 35 (2000) 1603–1614.
[32] J.M. De Paoli, J.A. Alonso, R.E. Carbonio, J. Phys. Chem. Solids 67 (2006) 1558–1566.
[33] J. Rodríguez-Carbajal, Physica B 192 (1993) 55–59.
[34] M. Onoda, Y. Ogawa, K. Taki, J. Phys.: Condens. Matter 10 (1998) 7003–7013.
[35] H.P.R. Frederikse, W.R. Thurber, R. Hosler, Phys. Rev. 134 (1964) A442–A445.
[36] N.F. Mott, Metal insulator transition, in: Metal Insulator Transition, second ed., Taylor & Francis, London, 1990.
[37] G. Lucovsky, J.W. Allen, R. Allen, Institut of Physics, London, 1979.
[38] G.V. Chandrashekhar, L.L. Van Zandt, J.M. Honig, A. Jayaraman, Phys. Rev. B 10 (1974) 5063–5068.
[39] D. Emin, Adv. Phys. 24 (1975) 305–348.
[40] J. Fontcuberta, B. Martínez, A. Seffar, S. Piñol, J.L. García-Muñoz, X. Obradors, Phys. Rev. Lett. 76 (1996) 1122–1125.
[41] J. Torrance, P. Lacorre, Ch. Asavaroengchai, R. Metzger, Physica C 182 (1991) 351–353.